NATIONAL
URANIUM
TAILINGS
PROGRAM

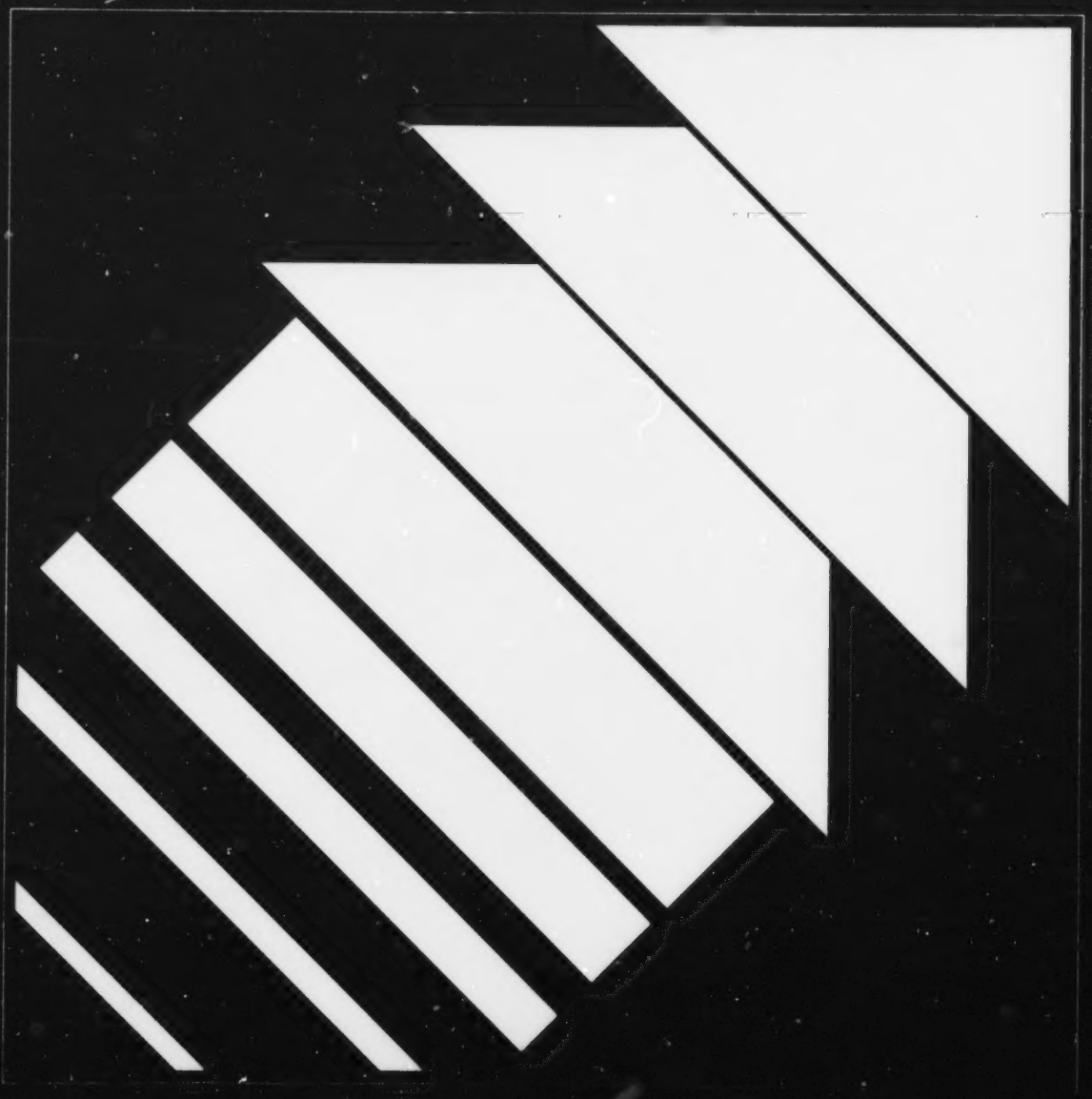

Canada

THE STUDY OF KINETIC CONTROLS ON PYRITE OXIDATION WITH APPLICATION TO ABANDONMENT OF PYRITIC URANIUM TAILINGS

THE STUDY OF KINETIC CONTROLS ON PYRITE OXIDATION WITH APPLICATION TO ABANDONMENT OF PYRITIC URANIUM TAILINGS

Final Report

Principal Investigators:
J.A. Cherry and R.W. Gillham

Research Associate:
R.V. Nicholson

A Research Report prepared for:
The National Uranium Tailings Program
Canada Center for Mineral and Energy Technology
Energy, Mines & Resources Canada
555 Booth Street
Ottawa, Ontario
K1A 0G1

WRI No. 310-07
DSS Ref. No. 20ST.23241-3-1664
Contract No. OST83-00341

INSTITUTE FOR GROUNDWATER RESEARCH
University of Waterloo
Waterloo, Ontario
N2L 3G1

MICROMEDIA

77pp

November, 1984

CONTENTS

SUMMARY ii

page

INTRODUCTION 1

EXPERIMENTAL 5

Materials 5
Methods 12
Pyrite and Silica Sand Preparation Procedure 12
Oxidation Procedures 15
Long Term Oxidation 16
Moisture Content Effects 17
Simulated Reaction Progress 21

RESULTS AND DISCUSSION 23

Long Term Oxidation 23
Moisture Content Effects 37
Simulated Reaction Progress 44

CONCLUSIONS 52

REFERENCES 55

Appendix page

A. SUMMARY OF DATA FROM THE LONG-TERM (SURFACE-AREA) EXPERIMENT (PYROX2). 56

B. SUMMARY OF THE DATA FROM THE SIMULATED REACTION PROGRESS EXPERIMENT (PYROX10) 63

LIST OF TABLES

Table		page
1.	Summary of the predicted values for the rate constants and the effective diffusion coefficients for the long term experiment.	35
2.	Summary of conditions related to the unsaturated cell.	40
3.	Cumulative fraction of pyrite digested.	46
4.	Average oxidation rates with standard deviations and number of data after each treatment by vigorous oxidation.	47
5.	Summary of sulphate concentrations and effluent weights for PYROX2.	57
6.	Summary of Flow Rate Data for the Preliminary Surface Area Experiment (PYROX2).	59
7.	Summary of Average Oxidation Rates for the Preliminary Surface Area experiment (PYROX2).	61
8.	Summary of the average flow rates for the PYROX10 series experiment	64
9.	Summary of the oxidation rates for the PYROX10 series experiment.	66

LIST OF FIGURES

Figure		page
1.	The moisture-suction-cup and the stainless-steel coil. (1) cylindrical wall, (2) Membrane, (3) Stainless-steel screens, (4) Rubber O-ring seal, (5) Bottom plate, (6) Effluent port, (7) Flushing port	6
2.	Schematic diagram of the Unsaturated Cell.	9
3.	A schematic diagram of the syringe column device	11
4.	A schematic diagram showing the arrangement of the experimental system for the long-term experiments.	18
5.	Operational design for the moisture content experiment.	20
6.	The observed oxidation rates versus time for the long term experiment. (a)- 54, (b)- 76, (c)- 108, (d)- 153, (e)- 215 microns.	24
7.	Oxidation rate versus the inverse grain size during the first 400 h of the reaction.	27
8.	Oxidation rate versus the inverse of the grain diameter squared after about 8000 h of reaction progress.	28
9.	Averaged rate versus time, (a)- 76 microns, (b)- 108 microns and (c)- 215 microns.	29
10.	The fraction of pyrite oxidized versus time for the three grain sizes.	31
11.	Representation of a shrinking core model (SCM) with the relative concentrations of reactant at and near the particle surface.	33
12.	Moisture content versus the pressure head observed for the unsaturated cell.	39
13.	Oxidation rate versus moisture content.	41

14. Oxidation rate versus the solution flow rate in the unsaturated cell experiment. 43

16. Oxidation rate versus the fraction of pyrite oxidized for data (points) and predicted (lines) values. 49

SUMMARY

A laboratory investigation was undertaken to further clarify the controls on pyrite oxidation in carbonate-buffered solution. The behaviour of oxidation rates over extended periods of time and reaction progress was examined. The effects of variation in localized moisture content in the presence of unlimited oxygen in the gas filled pores was also studied. Flow through systems were used in which granular pyrite or silica sand and pyrite mixtures were maintained under partially-saturated moisture conditions. Gas with atmospheric levels of oxygen was also passed continuously through the samples.

The results of oxidation runs that had been on-going for about 10 thousand hours were compared to predictions of a model based on shrinking core theory. Over extended periods of time, the rate of pyrite oxidation in a dilute alkaline environment decreased by a factor of two or more with time. Experimental evidence suggests that over the course of about one year, resistance to oxidation increases as would occur if a reaction coating were formed on the pyrite surface. When compared to the theoretical behaviour expected for such a process, only slight deviation is observed for the experimental data. The deviation tnat does occur, however, suggests that the formation of the reaction coating may not be complete or that some of this coating redissolves with time. This results in oxidation rates that are intermediate between those expected for reaction control only and those that are expected when diffusion through the reaction layer is dominant. Because the reduction in rates over the 10 thousand hour experiment was significant, it would seem to be important to include some means of estimating the rate change if predictions of oxidation rates in natural systems are required.

Extended reaction progress of three separate grain-size fractions was simulated. Stages of vigorous oxidative treatment that were used to simulate extended reaction progress resulted in spurious behaviour of the oxidation in the alkaline solution. In one case, the surface area probably increased during treatment while in another, the reaction rate not only decreased significantly but the observed rates suggest that a surface coating formed. The results do, to some extent, reflect behaviour predicted by the shrinking core model.

The effect of moisture content variation on oxidation rates was studied with the use of an unsaturated cell in which it was possible to control and maintain specified moisture content conditions while monitoring the rate of oxidation. The results of the experiment involving the unsaturated reaction cell show that the changes in local moisture content do not affect the rate of oxidation when oxygen is in continuous supply. This lack of observable effects suggest that changes in moisture content was not an important factor in previous experimental runs. Although there was some correlation between oxidation rate and solution flow rate in this experiment, it was shown earlier that this is not an important factor when flow rates are in the higher range of values that were associated with nearly all previous experiments.

INTRODUCTION

The hydrogeology research group at the University of Waterloo has conducted a number of field investigations related to the contamination of subsurface pore-water within inactive uranium tailings at Elliot Lake. It is evident from those studies that pyrite oxidation in the shallow subsurface followed by migration of the affected pore water is responsible for the presence of low pH pore-water within the tailings mass and in some areas within the sandy deposits underlying the tailings. In addition, high concentrations of dissolved iron and sulphate in the tailings pore-water are a direct result of the oxidation process. Levels exceeding those of drinking water standards of many metals and some radionuclides such as U, Th, and ^{210}Pb, are also related to the oxidation of pyrite in that the solubilities of many mineral phases containing those substances are generally enhanced at low pH.

The present practice of tailings management at inactive sites consists of establishing a grass cover after an application of small quantities of crushed limestone and fertilizer. It is evident that this treatment does not prevent pyrite oxidation and concomitant acidification of subsurface pore-water. If further remedial action is not

taken to prevent rapid pyrite oxidation, both in tailings that are presently inactive and at currently active sites, contamination will continue to occur, giving rise to potentially severe long-term environmental effects.

Recognizing the importance of pyrite oxidation in the geochemical evolution of tailings pore water, it is evident that an understanding of the kinetic factors that control the rate of oxidation and subsequent acid generation is essential to evaluating the long term environmental effects of the tailings deposits. The ultimate objective of the study of pyrite oxidation is to determine what conditions are necessary to minimize the flux of acid and other reaction products into the tailings pore water. To attain this goal, it is necessary to understand the kinetic controls involved in this reaction and subsequently to predict, over extended periods of time, the pore water chemistry and pH as they relate to possible alternative engineered characteristics of the uppermost zone of the tailings mass after abandonment.

Previous studies that, we have completed have shown that although it is favourable to maintain near-neutral conditions in an attempt to minimize rates of pyrite oxidation, other variables such as temperature, available surface area and especially oxygen concentration are also important and influence the kinetics of this reaction. The results of these rather short-term laboratory experiments,

however, may not strictly apply to the actual behaviour over extended periods. In addition, there has been some question as to the possible role of moisture content (the amount of water filling the pores) on the rates of oxidation observed in the experiments involving sandy pyritic-samples that were partially water-saturated. Further study was therefore desirable to gain an understanding of potentially significant controls on pyrite oxidation over the long term as well as to assess the possible role of moisture content on the rates of oxidation observed in previous experiments.

The purpose of this study was two-fold. The first aspect concerned the identification of controlling factors over extended periods of time. The second aspect was to determine the influence of localized moisture content variations on the rates of oxidation when unlimited oxygen is available in the gas phase.

Laboratory column and leaching experiments were designed to address these goals. The long term behaviour affecting pyrite oxidation was assessed in two ways. During preliminary experiments, a number of columns containing pyritic sand were leached with dilute $NaHCO_3$ solution in a manner that has been described in a previous report (Cherry et al., 1983). After completion of the initial project, the samples was continued to be leached giving a total monitoring period in excess of one year. With financing from the present study, the later samples were analysed and

the data was processed to determine oxidation rates over this period. In addition to this, a rapid leaching experiment was designed to simulate the long-term oxidation of pyrite with measurement of the rates of oxidation by dilute $NaHCO_3$ solution at intermittent stages of treatment.

The effect of moisture content on the rate of oxidation was examined in a separate experiment that involved a specially designed unsaturated cell. This cell had membranes at the ends that allowed passage of water but not air. The pyritic sand that was packed between the membranes was leached by $NaHCO_3$ solution while maintaining a constant flux of oxygen through the pore spaces in the sand. The moisture conditions in the cell were then varied in stages to observe the rate of oxidation at the various levels of moisture content.

EXPERIMENTAL

Materials

Pyrite was obtained from Wards Scientific Co. as aggregates of euhedral crystals or relatively pure massive specimens. The variety used in these experiments originated in Rico, Colorado. Because mixtures of sulphide minerals interact electrochemically during oxidation, pure pyrite specimens were desirable. Ottawa sand was used for experiments that involved pyrite-sand mixtures.

The leaching solutions used in all experiments consisted of double-deionized water containing 5 mmol L^{-1} of $NaHCO_3$. Specially prepared and analysed compressed-gas mixtures were used to control the oxygen concentrations in two of the experiments. These gas mixtures contained 0.5% CO_2 by volume. Because of the large volumes of gas needed, compressed air was used for the experiment to simulate reaction progress.

Three types of reaction vessels were used. The choice of apparatus was based on the level of control needed for each experiment. The experimental conditions in these experiments included 1) continuous solution flow; 2) maintenance of unsaturated conditions (pore spaces only partially filled with solution); and 3) continuous gas flow through the porous material.

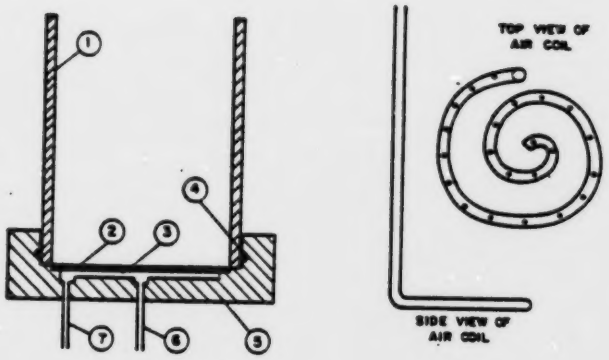

Figure 1: The moisture-suction-cup and the stainless-steel coil. (1) cylindrical wall, (2) Membrane, (3) Stainless-steel screens, (4) Rubber O-ring seal, (5) Bottom plate, (6) Effluent port, (7) Flushing port

The apparatus used in the long term experiment is referred to as a "moisture-suction cup" (see Fig. 1). The moisture-suction cup was constructed from an 8 cm length of 57 mm ID Plexiglas(R) cylinder with a base plate containing an Acropore(R) filter membrane (8 micron pore diameter) and two stainless steel tubes (2 mm ID) through the bottom of the plate. The effluent line consisted of a two metre length of plastic tubing attached to the centre tube of the base plate. The pressure head at the porous membrane was adjusted by positioning the end of the tubing at the desired level below the cup. The other steel tube was used to remove gas, by back-flushing the bubbles that accumulate below the membrane. Gas flow within the pyritic-sand bed was provided through the perforations in a coiled stainless steel tube that was positioned in the sandy material when the cup was filled. The gas exits through the porous sand into the atmosphere. This design was chosen because it was relatively uncomplicated and contamination by atmospheric oxygen was not a problem. Oxygenated gas was continuously passed through the pyritic sand and negative water pressure was maintained through the porous membrane.

The experimental apparatus used in the study of moisture content effects is referred to as an "unsaturated reaction cell". This cell was designed to control moisture content with uniform conditions throughout the porous material that is placed within the cell. Allowance was also made to

introduce a flow of a specified gas through the cell while preventing atmospheric contamination.

The cell was constructed from plexiglas(R) with a rectangular interior cross-section of 70 x 21 mm and a length of 85 mm (Fig. 2). Top and bottom endplates were fitted with membranes (8 micron pore diameter) that allow water but no air to pass at moderate to low pressures. Each endplate was fitted with two stainless steel tubes (2 mm ID) providing a means to flush the space adjacent to the membrane with the desired solution. One tube in each plate was connected to one metre lengths of tubing with the top-plate receiving the influent solution and bottom plate discharging the effluent. These tubes were also used to control pressure head at the membranes by adjusting the heights of the solution-filled tubes. Gas is introduced through a perforated plate in the broad side of the cell and exits through the opposite side through a similar plate.

An alternative experimental system was designed for oxidation experiments involving intermittent acid leaching and processing of replicate samples. Less control on environmental parameters was needed while maintaining consistency between experimental units. Each unit was constructed from a 10 cm^3 plastic syringe containing a bottom layer of glass wool overlain by a coarse paper filter and a rubber O-ring (Fig. 3). Solution and air entry were provided through ports at the top of the syringe. Solution

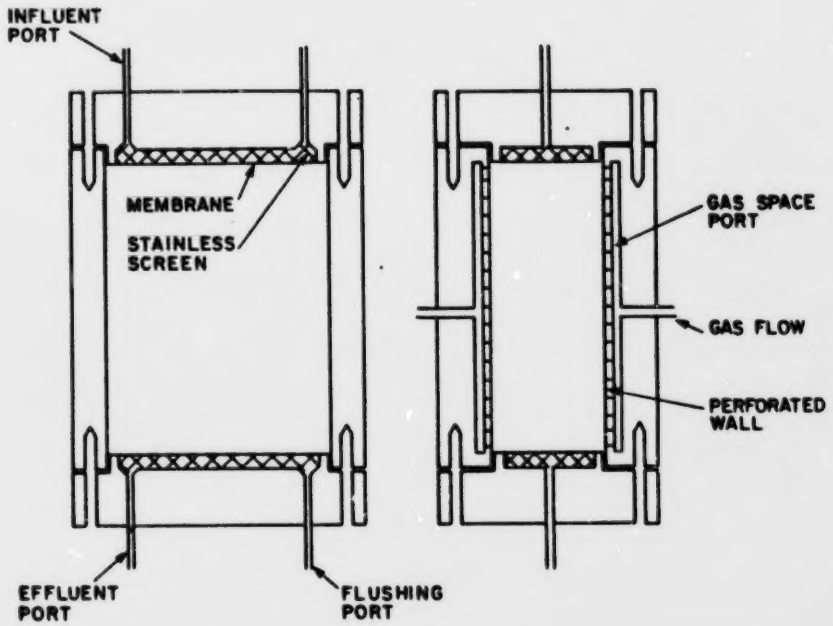

Figure 2: Schematic diagram of the Unsaturated Cell.

flow rates were drop controlled while rapid gas flow was induced by positive pressure above the granular pyrite specimen. Both solution and gas phases exited through a tube at the bottom of the syringe where the solution phase was collected. Six units were run simultaneously with both solution and compressed air delivered through their respective manifold systems. The positive gas pressure insured that the pyrite sample remained only partially saturated during the experiment.

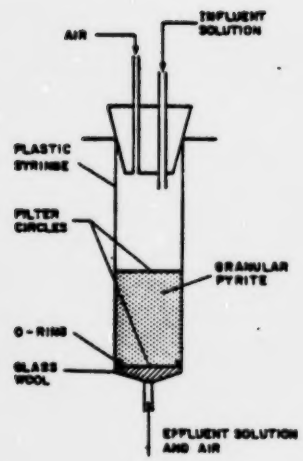

Figure 3: A schematic diagram of the syringe column device

Methods

Pyrite and Silica Sand Preparation Procedure

Crushed granular material was used in these experiments to enhance the surface area available for oxidation. Because surface area was one of the variables being investigated, it was necessary to insure that its value remain constant during the runs involving different levels of the other variables. In addition, an estimate of the surface area was needed. Surface area can be measured or estimated by different methods. Although it is desirable to have measured values of this variable in kinetic studies, the low values of surface areas (approx. 10^{-2} m^2g^{-1}) associated with the selected grain-size diameters used in this investigation were below detection with available equipment (N_2 adsorption-BET). The estimation of surface area was therefore based on representative grain diameters. For this reason, special care was taken to insure uniform grain-size within narrow limits.

It is known that after crushing pyrite, ultra-fine material electrostatically adheres to the surfaces of the coarser grains. On a unit weight basis, these fines represent a much greater surface area than that associated with the coarser grains. If the fine material is not removed, rapid oxidation is likely to occur initially due to the greater available surface area, after which the reaction rate would decrease as many of the fine particles dissolve

completely. This phenomenon is similar to that postulated to occur in feldspar-dissolution experiments at short times (Holdren and Berner, 1979). In this case, the reaction rate would be affected by changing surface area and would introduce errors in the estimation of rates based on different levels of the other variables. Proper cleaning is therefore necessary to minimize this source of uncertainty.

The pyrite specimens were obtained as large (0.5kg) crystalline masses. After breaking the larger pieces with a hammer, the pyrite was mechanically crushed between ceramic plates to a diameter of about 2 to 10 mm. Initially this material was then pulverized with a mortar and pestal until sufficient fines were present to collect the desired size-fractions. A benchtop ceramic ball mill was later used in place of the mortar and pestal. About 80g portions of the pulverized pyrite were sieved on each run. Sieving was performed on a Rototap shaker with six stainless steel screen pans (60,80,120,170,230 and 325 mesh-Tyler) for 15 minutes per run.

Each size fraction was subjected to a washing procedure. Up to about 100g of sieved pyrite was placed in a beaker followed by about double the weight of deionized water. The contents of each beaker were mixed thoroughly with a rubber-tipped stirring rod and, after allowing the main size fraction to settle, the supernatant was discarded. This procedure was repeated until the supernatant solution was

clear and colorless. The beaker containing the pyrite and water was then immersed in an ultrasonic cleaner for 45 seconds. Washing was then repeated until the supernatant appeared clear and colorless. After allowing the water to drain, reagent-grade acetone was added to the pyrite. The contents were stirred and the overlying liquid was discarded. This procedure was repeated until the acetone was clear and colorless. After decanting the final acetone rinse, the beaker was placed in a dessicator and a vacuum was applied. When the pyrite was dry, each sample was resieved through the appropriate mesh interval. In this way the fine-grained pyrite that was present in the initial unwashed fraction was removed.

The resieved sample was then rewashed with water to remove the small amount of fines produced during sieving. After decanting the last water rinse, a similar volume of 6N HCl was added to the pyrite. The acid wash removes the small amounts of ferric hydroxide precipitate that adhere to the pyrite surface after slight oxidation. The contents of the beaker were stirred thoroughly and allowed to stand for about 10 minutes. Further water washing was performed to remove the HCl and a final two washes with acetone were made. The sample was then stored under vacuum in a dessicator. The pyrite samples designated for the oxidation experiments were treated only a few days before use.

The sized silica sand was prepared using Ottawa sand that consisted of well rounded quartz with most grains originally larger than 60 mesh. The sand was pulverized in a ceramic ball mill in preparation for sieving. The sieving procedure was similar to that used for the pyrite. The selected size-fractions were washed by passing deionized water through a 1.5m length of acrylic cylinder (5cm ID) containing about 1kg of sand. The flow-rate was adjusted so that the fines would pass through the top overflow port while the main size fraction remained suspended in the column. When the overflow water was clear, the washed sample was removed. This sand was then added to 8N HNO_3 and after mixing was allowed to sit for 2 to 3 days. The acid rinse was used to remove reactive impurities that may occur with the silica sand. After decanting the acid, water washing was repeated until the pH of the overflow water approached a value of about 6. The sand samples were then air dried and retained for later use.

Oxidation Procedures

Three separate experiments were conducted to study the influences of different variables on the rate of pyrite oxidation. A surface-area experiment involved separate runs, each containing one of five different grain-size fractions. The grain diameters, corresponding to the mid-point of the sieve-screen mesh interval, were 215, 153, 108,

76 and 54 microns. These units were monitored for a period in excess of one year and the data was used to determine the effects of long-term oxidation. A second experiment involved the treatment of pyrite samples to vigorous oxidation. The oxidation rates after each treatment were determined in dilute alkaline solution. Three different grain sizes were used in duplicate. The moisture content study involved the use of one experimental unit. The unsaturated reaction cell (UC1) containing a pyritic sand mixture was subjected to conditions of varying moisture content while collecting data on the oxidation rates.

Long Term Oxidation.

Mixtures of pyrite and silica sand were loaded into the moisture-suction cups (Fig. 1) with the gas-delivery coil at the base of the sand. The sand was wetted with the influent solution through the effluent tube at the base of the cup. The saturated sand was then drained to equilibrium by placing the effluent tube outlet at a specified elevation below the cup. Based on moisture-drainage curves determined previously, the head level for each grain size was adjusted to give a volumetric water content of about 0.2. A coarse paper filter was placed on the surface of the sand to spread the influent solution that was added dropwise at a rate of about 10 mL h^{-1}. Flow of the gas phase was then adjusted to about 1200 mL h^{-1}. In the runs involving surface area and temperature, the gas phase was allowed to exit at the top of

the cup into the atmosphere. The design of the flow system is shown in Fig. 4.

The solution-flow rate could not be held constant over time because of poor control on the drop rate. Therefore, a total mass balance was maintained on the sulphate eluted from each cup. The effluent solution from each unit was collected in pre-weighed flasks. The effluent was weighed and a sample was collected daily or more often and retained for later analysis of sulphate. The pH of the influent and effluent solutions were also monitored periodically.

Moisture Content Effects.

The unsaturated reaction cell was packed with a silica sand mixture containing 20.0 g of pyrite (215 micron diameter) and approximately 180 g of silica sand with the same grain size. The membranes were wetted with the $NaHCO_3$ solution and then the short lengths of plastic tubing that were attached to the stainless steel tubes were clamped so that the entire unit could be weighed before significant wetting of the sand occurred. After weighing, the influent and effluent tubing were attached to the upper and lower endplate respectively. The $NaHCO_3$ solution was added to the sand within the cell from the bottom upward. After wetting, the cell was detached from the inlet and outlet tubing and clamped so that the weight of the saturated sand could be measured. This provided an estimate of porosity and moisture content.

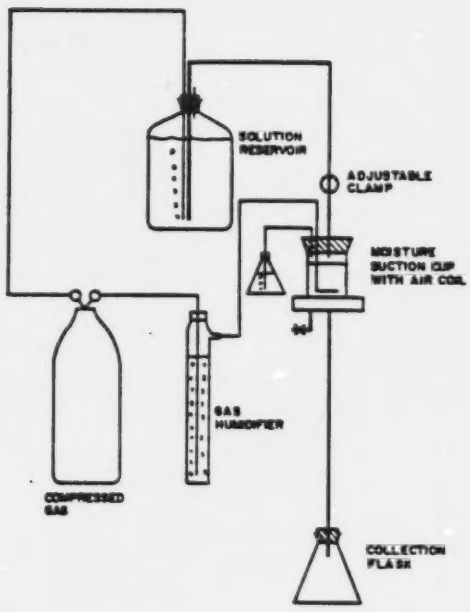

Figure 4: A schematic diagram showing the arrangement of the experimental system for the long-term experiments.

The pressure heads in the influent and effluent end plates were then adjusted to obtain a unit gradient (i.e. elevation head difference equal to the actual vertical distance between the membranes). The relative pressure head at each endplate was set at a slightly negative value so that the sand did not remain completely saturated. A Marriot syphon was used to maintain a constant pressure at the influent membrane while the pressure at the effluent membrane was controlled by the elevation of the hanging water column in the attached tubing. Gas flow was provided from a compressed gas cylinder and the flow rate was monitored and maintained at about 1.5 L h^{-1}. The operational design of the experimental system is shown in Fig. 5

After initiating solution flow through the column, the flow rate was lowered somewhat by restricting the inflow of solution through the influent tubing. Because flow rate decreases with decreasing saturation (at unit gradient) and because it was intended to lower the degree of water saturation without significantly altering other variables, an attempt was made to maintain a consistent solution flow rate throughout the experimental run. The effluent was collected, weighed and analysed for sulphate concentrations in the same manner as discussed previously.

After collecting data for several days and observing relatively steady flow rates, the unsaturated cell was again

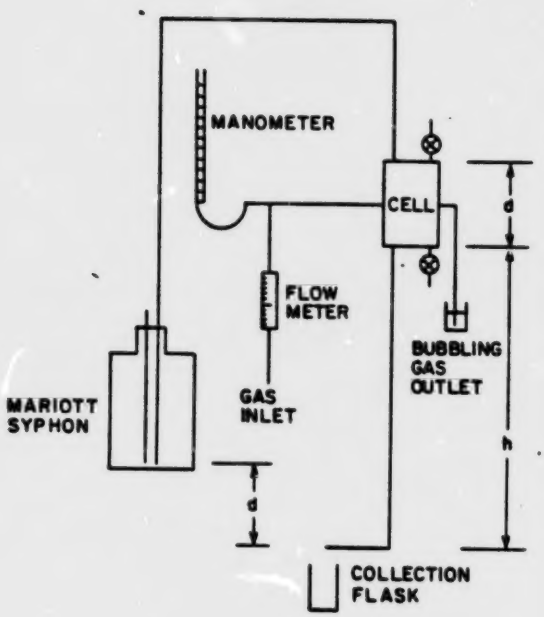

Figure 5: Operational design for the moisture content experiment.

disconnected from the inlet and outlet tubing and clamped. The weight was recorded and the moisture content that corresponded to the specified pressure head was determined. The cell was reconnected to the solution and gas lines and then the pressure heads at the two endplates were lowered by an equal amount. The decreased pressure head setting resulted in a lower equilibrium moisture content. Effluent was collected over several more days and the process was repeated. This resulted in the observation of oxidation rates at various moisture content values in the range from near saturation to about 50% of saturation.

Simulated Reaction Progress.

The syringe leaching device was used in this experiment. Two replicate units of each grain size were prepared. Each unit consisted of 10 g of the specified pyrite with a pair of replicates having grain diameters of 215, 108 and 54 microns. Solution and gas flow were delivered to each syringe unit through outlets from a manifold designated for each phase. The influent solution was added dropwise at a rate of about 10 mL h^{-1}. The total gas flow was adjusted to about 70 L h^{-1}, which resulted in measured gas pressures above the pyrite equivalent to about 1.4 to 2.0 m of water. The effluent solution from each unit was weighed and collected in the same manner as noted above. This experiment was maintained at an ambient room temperature of $23 \pm 2\ ^{o}C$.

After a specified number of days, the pyrite samples that had been oxidized under weak-alkaline conditions were then treated under extremely oxidizing conditions. Each syringe unit was removed from the flow system and about 10 mL of a mixture of HNO_3 + HCl + Br_2 (3 + 1 + 0.02 approx.) diluted with 10 mL of water was passed through the pyrite specimen. This solution was found to oxidize the pyrite significantly over a short period while allowing some control over the extent of reaction. The acidic solution was introduced to the pyrite in 5 mL aliquots to prevent uncontrolled behaviour of this highly exothermic reaction. The pyrite was later rinsed with HCl (6N) and finally with deionized water. All of the effluent was collected volumetrically and analysed for total dissolved iron by Atomic Adsorption Spectrometry.

The amount of pyrite leached during each treatment was determined from the total mass of iron in the acid effluent. After all units had been treated in this manner, they were replaced in the original flow system and again exposed to mild oxidation under dilute alkaline conditions. The complete process was repeated after sufficient data were collected to observe the rate of oxidation between treatments. In this way, the effects of long term reaction were simulated in a short period of time. Five treatments were applied over a two month period.

RESULTS AND DISCUSSION

Long Term Oxidation

Data was collected from the experimental units between December 1, 1982 and January 16, 1984. Dilute $NaHCO_3$ solution was continually passed through the pyritic sand at rates of about 0.01 Lh^{-1}. Compressed air flow was also maintained during the experiment. The temperature of the units were about 25 $\pm$ 2^{o}C over the long term. Samples were collected daily in the beginning of the experiment but were later collected weekly or bi-weekly. Occasionally, flooding of units due to poor drainage or significant spills due to unregulated high flow rates occurred. The affected effluent samples were noted but not analysed or used in this study. A summary of the data including sulphate concentrations, effluent weights, average flow rates and rates of oxidation appears in Appendix A.

The oxidation rates as a function of time are shown in Fig. 6 (a to e) for the different grain-size fractions. A fair degree of scatter is evident in the data. Some units exhibit observably less variability than others. In general, however, it is observed that the rates decrease with time over the approximately 10 thousand hour period.

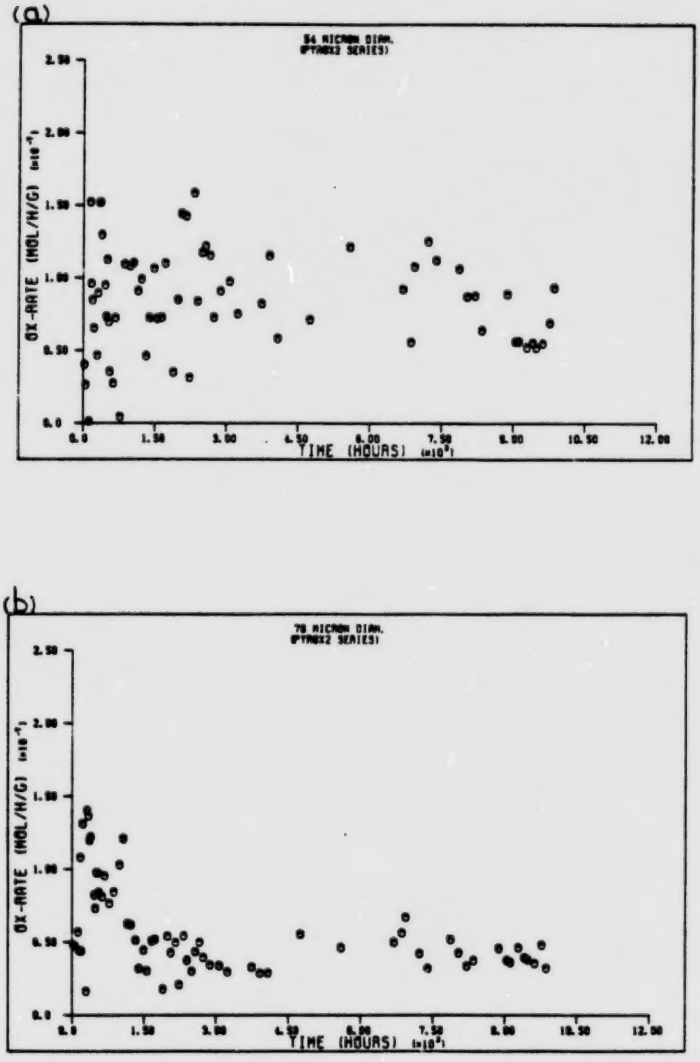

Figure 6: The observed oxidation rates versus time for the long term experiment. (a)- 54, (b)- 76, (c)- 108, (d)- 153, (e)- 215 microns.

(c)

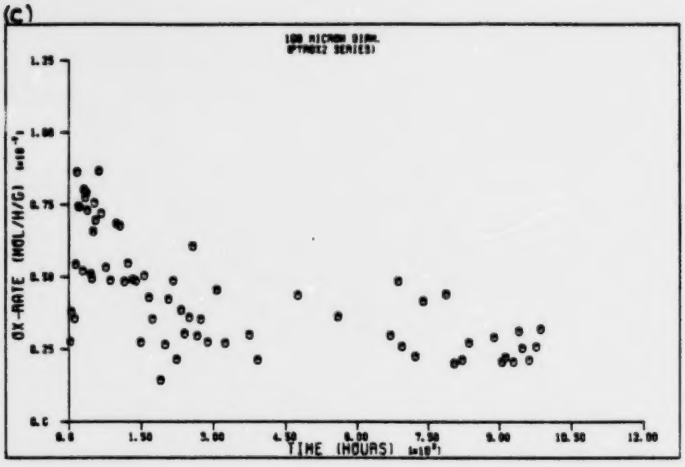
100 MICRON DIAM.
OX-RATE (MOL/M/G) (x10⁻⁴)
TIME (HOURS) (x10³)

(d)

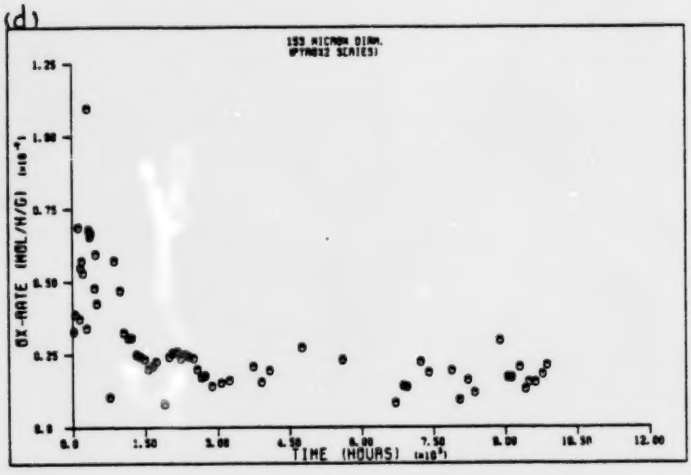
153 MICRON DIAM.
OX-RATE (MOL/M/G) (x10⁻⁴)
TIME (HOURS) (x10³)

(e)

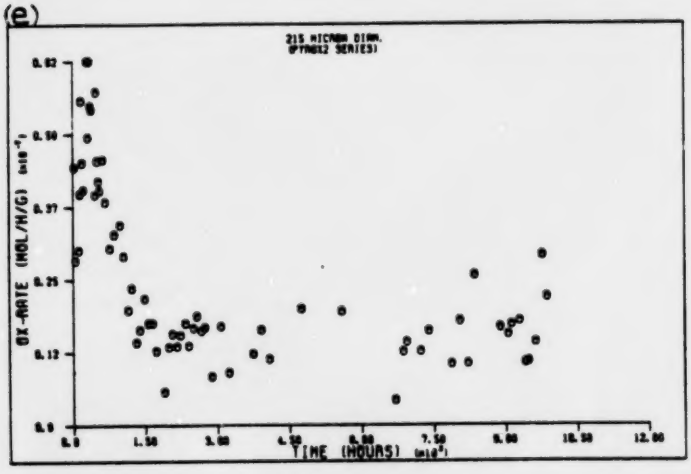
215 MICRON DIAM.
OX-RATE (MOL/M/G) (x10⁻⁴)
TIME (HOURS) (x10³)

Initially, these experiments were designed to study the effect of surface area on the rate of pyrite oxidation. Surface area measurements were not conducted because of the small values for this parameter but estimates were acquired from the relationship between surface area and particle grain size assuming that a spherical shape would be representative. The relationship can be expressed as;

$$S = 3M/pd \qquad (1)$$

In which S is the total surface area, M is the mass, p is the particle density and d is the diameter of the particles. This shows that the surface area is inversely proportional to the particle diameter and hence 1/d is used here as an estimate of the former.

A plot of oxidation rate versus the inverse diameter for each of the grain size fractions at early times indicates that the relationship is linear (Fig 7). However, at times greater than about 8000 hours a linear relationship is observed between the rate and $1/d^2$ (Fig. 8). These observations indicate that the processes controlling the rate of oxidation have changed with time. In the early stages, the linear relationship that is implicit between rate and surface area indicates that the rate is surface controlled by the reaction rate constant. The later change to a linear dependence on $1/d^2$ suggests that the rate was then controlled by the development of a coating or reaction

layer on the pyrite surfaces. These relationships are discussed mathematically by Levenspiel (1972, Chap. 12).

Three grain-size fractions that appeared to exhibit lesser degrees of scatter were chosen for further analysis. These include the ones with particle diameters of 215, 108 and 76 microns. Smoothed versions of the rate versus time relationships were obtained by calculating the moving average (15 consecutive data points) and the resulting curves are shown in Fig. 9 (a to c). The area under each curve was then integrated to find the accumulated amount of pyrite oxidized with time. The result of these calculations is shown in Fig. 10 (a to c) as the fraction of pyrite oxidized versus time. The results show that the maximum amount of pyrite leached varies from about 2% for the coarse grain size to about 5% for the fine grain size over nearly 10 thousand hours. The response is also observed to be non-linear in contrast to a linear behaviour that would be expected if the rates of reaction had remained constant. The fact that oxygen was in continual supply and the solution flow rate and temperature did not change significantly with time, provides additional evidence that some time-dependent process has resulted in the observed decreases in oxidation rates.

During pyrite oxidation, ferrous iron is released and oxidized to ferric iron. At neutral to alkaline pH levels, the ferric iron will form a hydrated precipitate (i.e.

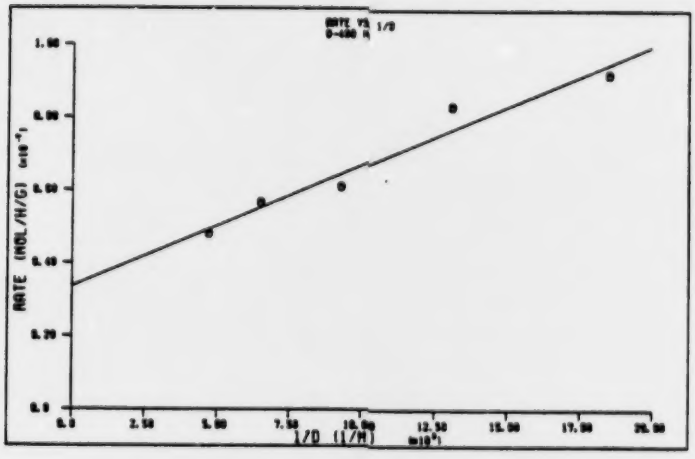

Figure 7: Oxidation rate versus the inverse grain size during the first 400 h of the reaction.

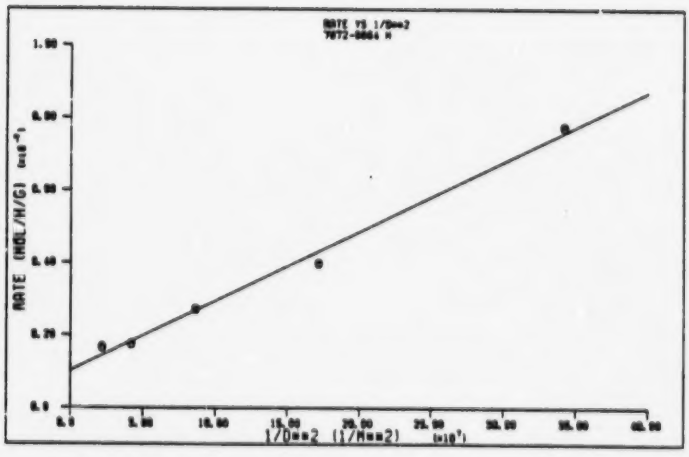

Figure 8: Oxidation rate versus the inverse of the grain diameter squared after about 8000 h of reaction progress.

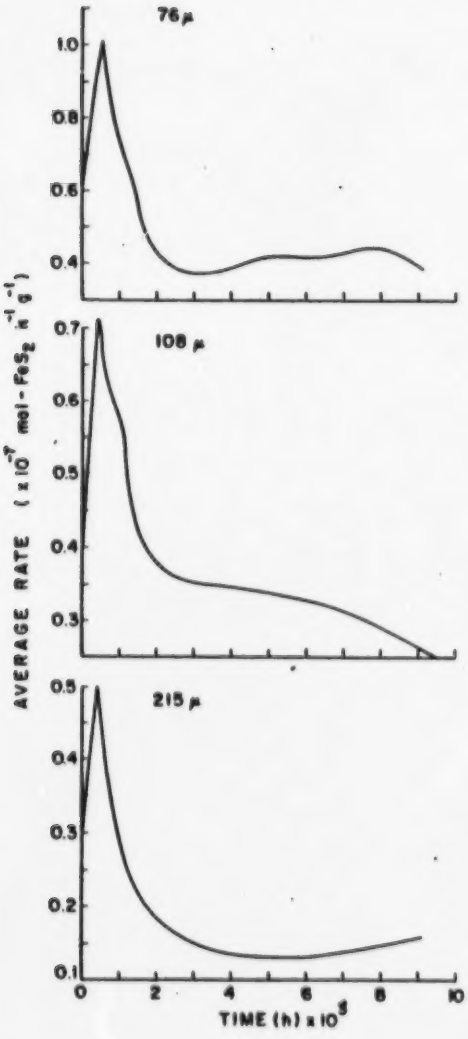

Figure 9: Averaged rate versus time, (a)- 76 microns, (b)- 108 microns and (c)- 215 microns.

$Fe(OH)_3$) and the rate of formation would be quite rapid under these conditions. If precipitation occurred before ferrous iron was released from the pyrite surface, then the accumulation of the precipitate on the pyrite surface is probable. This oxide coating would impede the transfer of oxygen to the fresh pyrite surface and thereby slow the reaction as the buildup of the coating proceeds. This would result in a continual decrease in the rate of pyrite oxidation with time. In a qualitative sense, this mechanism appears to be supported by the results shown in Fig. 10 (a to c), in which the rate of increase of total pyrite oxidized decreases with time. To further evaluate this hypothesis, the results were compared with predictions of a simplified model of reactive dissolution with formation of a reaction coating ("shrinking core model" -SCM).

Levenspiel (1972) presents the development of the mathematics involved in the SCM. Beginning with a simple geometric form of a particle, it is assumed that at any time the reaction is controlled by both steady-state diffusion of the reacting gas through the reaction coating that develops on the particle surface and the surface rate constant (Fig. 11). It is implicitly assumed that the core shrinks at a much slower rate than is needed to attain steady state concentration conditions across the reaction layer. The two controlling processes act as resistances to the rate of reaction and effectively are additive in sequence. The time

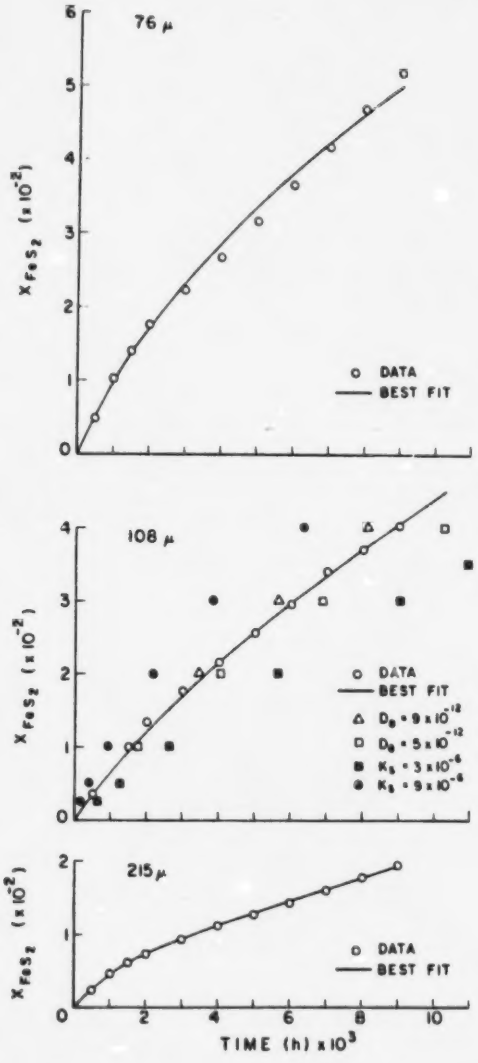

Figure 10: The fraction of pyrite oxidized versus time for the three grain sizes.

dependence of the amount of pyrite oxidized can then be determined by including such parameters as the reaction-rate constant and the effective diffusion coefficient for oxygen through the reaction coating. The equation can be expressed in the following way;

$$t = [R^2/(6bD_eC)]\ [1-3\ (1-X)^{2/3} + 2(1-X)] + [R/(bk_sC)]\ [1 - (1-X)^{1/3}] \quad (2)$$

in which t is time, p is the molar density, R is the initial particle radius, b is the stoichiometric ratio between pyrite and oxygen, C is the concentration of oxygen, k_s is the rate constant, De is the effective diffusion coefficient and X is the mole fraction of the original pyrite that has oxidized.

The results of this model were compared to the data and a "best visual fit" was obtained. Both k_s and De were determined in this manner. As shown in Fig. 10b, the model is rather sensitive to small changes in either one or the other of these parameters. In this example, two values of D_e were chosen to bracket the best-fit value while k_s is held at the best-fit value. The two values for k_s were chosen similarly. However, for this particular model, the response at early times is most sensitive to changes in k_s whereas at later times the sensitivity increases to changes in De. A fairly good fit was obtained for all three grain size fractions. These findings support the initial

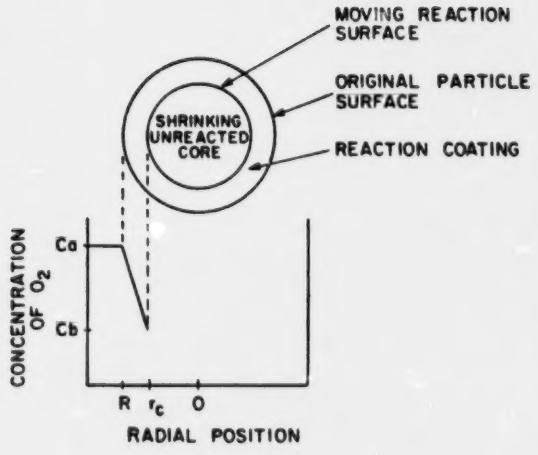

Figure 11: Representation of a shrinking core model (SCM) with the relative concentrations of reactant at and near the particle surface.

hypothesis that a reaction coating is forming on the pyrite surfaces with time.

As shown in Table 1 the values of k_s that were determined from the model are rather consistent. Maximum differences are less than 45% of the meon value. The values of De are also quite consistent with maximum relative differences of about 60%. The values for the effective diffusion coefficients are about six orders-of-magnitude less than those observed through pure water but are also 2 to 7 orders-of-magnitude greater than those for ions diffusing through highly structured solids. Because a precipitate such as $Fe(OH)_3$ is often a poorly structured amorphous substance it may behave somewhat as a porous substance. If this is the case, it is not surprising that the effective diffusion coefficient for this material is intermediate between those of water and more structured solids. Because not all of the surface coatings are expected to develop uniformly, it is also not surprising that the effective diffusion coefficients would vary somewhat. In that diffusion coefficients in solids can vary over five or six orders-of-magnitude, the one-order-of-magnitude difference found here is not great.

There is, however, some deviation from the model prediction at later times. This lack-of-fit can be observed for data representing the fine-grained pyrite in Fig. 10a in which the predicted fraction of pyrite oxidized falls short

TABLE 1

Summary of the predicted values for the rate constants and the effective diffusion coefficients for the long term experiment.

Grain Size (microns)	k_s ($m\ h^{-1}$)	D_e ($m^2\ h^{-1}$)
215	8.9×10^{-6}	2.7×10^{-12}
108	4.5×10^{-6}	6.6×10^{-12}
76	5.2×10^{-6}	3.3×10^{-12}

of the actual amount after about 6000 h. A similar trend is observed for the coarse-grained pyrite shown in Fig. 10c, but only after about 9000 h. The data representing the intermediate grain size does not exhibit any consistent lack-of-fit over the entire 10,000 h period.

The reasons for deviation of the data from the model predictions are not known but may be attributable to several recognized uncertainties. First, it is likely that not all oxidized iron will form a continuous coating on the pyrite surfaces. Some Fe^{2+} or Fe^{3+} will undoubtedly escape to solution where it could then precipitate either suspended in solution or on other solid material. This "loss" of reaction coating would result in less resistance to the oxidation reaction and hence the quantity of pyrite oxidized would exceed the predicted amount with time. Second, the precipitate that is formed by ferric hydroxide would dissolve slowly with time. Although the equilibrium solubility of this material is low at pH levels of about 7 (approx. 10^{-8} mol L^{-1} total Fe(III)), continuous leaching by the influent solution would slowly remove the outer layers of the precipitate. Because the model does not account for this loss, deviation of the data from the model results would occur in a manner similar to that observed here. Third, the oxide layer is not thermodynamically stable on the surface of the sulphide mineral. Some partial redox reactions would be expected, possibly resulting in the

release of some of the oxide components. This would result in some loss of the reaction coating with consequences similar to those discussed above.

Regardless of the reasons for deviation from the predicted behaviour, the close fit of the data over most of the 10,000 h experimental period strongly suggests that the formation of oxide coating is significant. This process results in decreases in the oxidation rates at early times by a factor of two or greater. This behaviour would not likely occur, however, in solution with low pH. Acidic conditions would increase the solubility of the oxide material and hence it is possible that precipitation of ferric hydroxide would not occur. Even in the neutral to alkaline environment, the evidence suggests that formation of the reaction coating is not complete and hence the oxidation rates over the long term will likely remain intermediate between those that would occur as a result of reaction kinetic control only and those that are controlled by diffusion through a reaction coating.

Moisture Content Effects

The dimensions of the cell and the physical properties of the pyritic sand within the unsaturated cell are summarized in Table 2. The total porosity and hence the saturated water content (expressed as the ratio of volume per total volume) was 0.40. This is a reasonable value for sandy

material. During the course of the experiment, the moisture content was adjusted from near saturation to about 50% of the saturated value (moisture content from 0.4 to about 0.2). The pressure head values relative to the membrane elevations varied from about minus 200 mm to minus 400 mm. A plot of moisture content versus pressure head is given in Fig. 12. Lower moisture content values were not attempted because flow rates were becoming so low that too great a time would have been required to collect a sufficient volume of effluent sample. Low flow rates result from the low moisture content conditions.

The oxidation rates were monitored over several days at a constant moisture content and the average rate over that period was plotted against its respective moisture content value. The resulting rates of oxidation occurring at various values of moisture content are shown in Fig. 13. No obvious relationship between oxidation rate and volumetric water content is revealed by the data. Although the moisture content values do not span the entire range of possible values, one would expect the range used in the experiment to be sufficiently large to reveal trends if any exist.

In contrast to the lack of observable relationships with the moisture content, there appears to be some influence on the rate of oxidation by the rate of water flux through the cell. Although an attempt was made to hold the solution

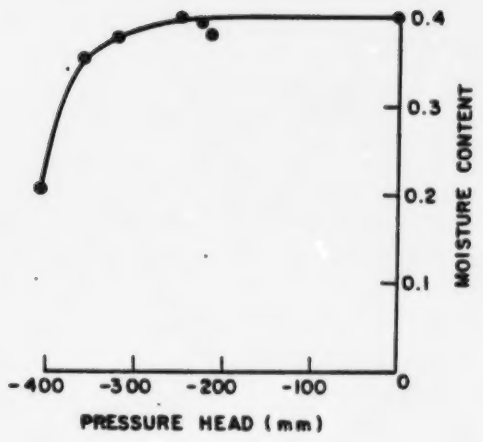

Figure 12: Moisture content versus the pressure head observed for the unsaturated cell.

TABLE 2

Summary of conditions related to the unsaturated cell.

Cross Sectional Area:	= 14.7 cm^2
Cell Volume	= 140.8 cm^3
Sand wt	= 225.6 g
Pyrite wt	= 20.0 g
Bulk Density	= 1.725 g cm^{-3}
Particle Density	= 2.87 g cm^{-3}
Porosity (n)	= 0.40

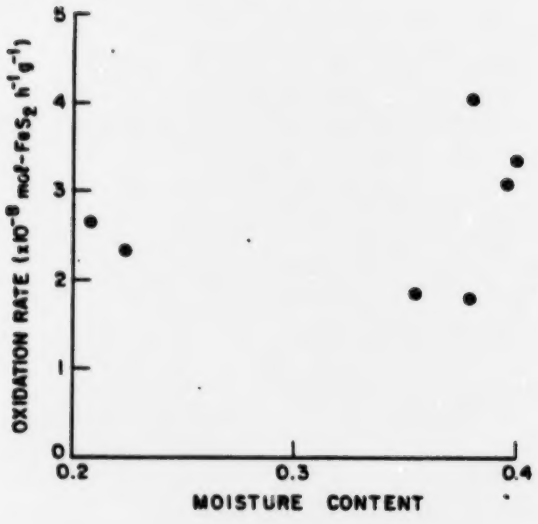

Figure 13: Oxidation rate versus moisture content.

flow rate constant, some variation occurred. A plot of oxidation rate versus the average flow rate is shown in Fig. 14. The data suggest that the oxidation rate increases with the rate of solution flow. This observation could result from either or both of two distinct processes, the effects of which cannot be distinguished here. These processes include stagnation of pore water and chaning film thickness for solution surrounding the pyrite particle.

One difficulty that arises in the use of cells or columns with flow through a porous medium, is that some zones of material may not be included in the flow process. These zones may be referred to as those containing dead-end pores or as stagnant. Although this is probably not a significant factor in systems that are fully water saturated, the extent of such zones is thought to increase at lower flux values, especially when the porous media becomes progressively drained. If this were the case, it is likely that the observed rates of oxidation would decrease as a result of the decreasing flow rates and increasing stagnant zones.

Alternatively, the changes in oxidation rate could be linked more directly to the velocity of solution in the medium. It is common in solid-aqueous reaction systems that water films result in diffusion control of reaction rates to lesser or greater extents. It is also known that increases in the velocity of water passing by the particle will decrease the effective thickness of the stagnant water film.

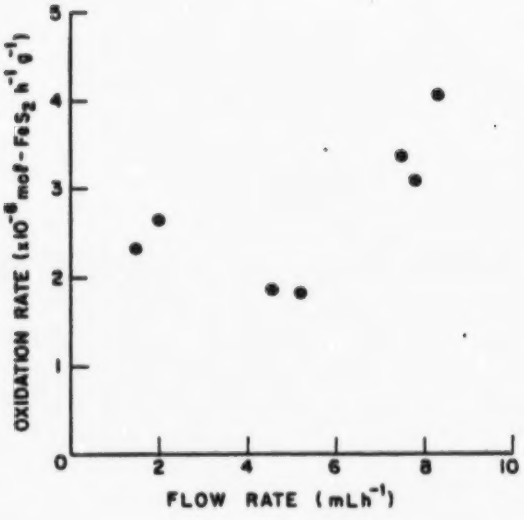

Figure 14: Oxidation rate versus the solution flow rate in the unsaturated cell experiment.

When this occurs, the resistance to diffusion of reactants (ie. O_2) would decrease and hence the rate of oxidation would increase to the limiting value set by the surface rate constant.

Previous experiments showed that oxidation rates are not affected by the solution flux values when the latter is in the high range. By necessity, the solution flux values in the present experiment remained low and hence influenced the rates of oxidation. In previous experimental runs solution flux was generally greater than those in this study by a factor of five or more. In that range, the slight variation in flow rates do not appear to influence oxidation rates. In addition, the present results suggest that variations in moisture content are not a factor in the rates of oxidation observed in previous experimental studies.

Simulated Reaction Progress

The three grain-size fractions were treated to vigorous oxidation for a total of five times each. Because some parameters such as temperature and rate of addition of the acidic bromine solution were not always constant during the procedure, the degree of oxidation was not always the same between grain-sizes or even between replicates. This lack of consistency, however, does not affect the comparison between predicted and observed results. The quantity of pyrite remaining after each treatment expressed as a

fraction of the original amount is given in Table 3. The quantity of pyrite oxidized after all treatments was in the range of 40 to 70% of the initial mass present.

The oxidation rates reported here are those observed under conditions of leaching by $NaHCO_3$ solution (0.005 mol L^{-1}) with atmospheric levels of both oxygen and carbon dioxide. The measured rates with their respective standard deviations and the number of measurements for each treatment are given in Table 4. In general, the rates of oxidation tend to decrease with time but increases after some treatments are evident. If a simple shrinking core model (SCM) is applied to these data, the rates would not be expected to increase.

The oxidation rates can be determined as a function of the fraction of pyrite oxidized for the SCM. For the case of surface controlled reaction with potential control by diffusion through a reaction coating, the relationship becomes;

$$-dN/dt = bS^{o}C/[R(1-(1-X)^{1/3})/(1-X)^{1/3}D_e + 1/(1-X)^{2/3}k_s] \quad (3)$$

in which all parameters are the same as those in (3) and S^{o} is the original surface area of the granular material. For reaction without diffusion, D_e is set at a large value.

TABLE 3

Cumulative fraction of pyrite digested.

	TREATMENT				
Unit	1	2	3	4	5
P10-1a	0.014	0.356	0.432	0.465	0.491
P10-1b	0.023	0.199	0.278	0.342	0.369
P10-2a	0.023	0.428	0.536	0.564	0.597
P10-2b	0.011	0.399	0.524	0.588	0.613
P10-3a	0.182	0.420	0.546	0.681	0.737
P10-3b	0.182	0.437	0.579	0.688	0.736

TABLE 4

Average oxidation rates with standard deviations and number of data after each treatment by vigorous oxidation.

Oxidation Rate (x 10^{-8} mol-FeS_2 h^{-1})
(Std. Dev./No. Data)

Treatment	P10-1a	P10-1b	P10-2a	P10-2b	P10-3a	P10-3b
0	1.76 (0.40/4)	1.82 (0.22/4)	5.26 (1.5/4)	4.09 (1.1/4)	12.0 (0.71/4)	10.8 (1.7/4)
1	1.66 (0.15/5)	2.42 (0.42/5)	4.60 (0.22/5)	4.29 (0.52/5)	5.99 (1.4/5)	5.76 (1.6/5)
2	0.94 (0.43/6)	1.98 (0.38/6)	1.99 (1.1/6)	0.96 (0.21/4)	2.90 (0.84/3)	3.05 (0.19/3)
3	1.07 (0.41/6)	1.96 (0.59/6)	2.95 (1.7/6)	2.96 (2.1/6)	4.82 (2.4/6)	4.31 (2.2/6)
4	1.68 (0.59/5)	2.64 (1.2/5)	2.12 (0.93/5)	2.10 (0.97/5)	2.65 (1.4/5)	2.71 (1.6/5)
5	1.60 (0.86/6)	3.00 (1.4/6)	2.53 (1.2/6)	2.02 (0.52/6)	2.48 (1.1/5)	2.71 (1.6/6)

The experimental results were compared to the rates of oxidation as a function of the fraction of pyrite leached as predicted from the SCM. The plots of rate versus fraction of pyrite leached are shown in Fig. 16 (a and b). Each of the grain size units appears to behave in a unique fashion with fairly good consistency between the two replicate samples of each size fraction. The solid lines in Fig. 16 (a) represent the predicted behaviour if only the surface chemical reaction controls the observed rates.

The coarse grain size unit (215 microns, Fig. 16 a) is characterized by slightly increasing rates of oxidation after almost every treatment, with rates after the final treatment that are anomalously greater than those observed before any treatment. The data for the intermediate grain size (108 microns, Fig. 16 a) exhibits general decreases after treatment with some oscillation evident. The observed rates are close to those predicted for reaction control after the fifth treatment. The data from the fine-grain-size (54 microns, Fig. 16 b) unit also exhibits a generally decreasing rate with increasing amounts of pyrite leached. The upper solid line on this plot represents the predicted behaviour for reaction only, while the lower line displays this relationship when diffusion through a reaction coating controls the rate of oxidation. In this case, the diffusion coefficient that was predicted for the surface coating was about 1.9×10^{-11} m^2 h^{-1}. This compares well with the

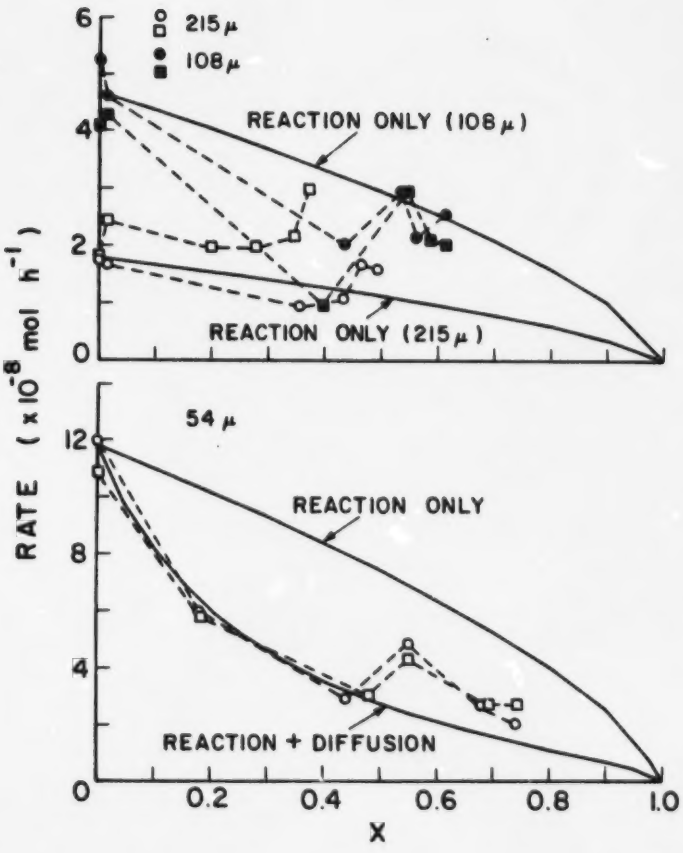

Figure 16: Oxidation rate versus the fraction of pyrite oxidized for data (points) and predicted (lines) values.

values of D_e predicted from the long term data above. The rates that were observed after the final treatment are intermediate in value between those predicted for diffusion control and those for reaction only.

With such inconsistency between units, it is difficult to interpret the present results. In general, it would be expected that any increase in oxidation rates would need to be accompanied by a corresponding increase in surface area. During the rapid oxidation of the coarsest grain-size fraction, this may have occurred. Why this appeared to occur only to the coarsest grain size is uncertain, but it may be that the larger particles are more susceptible to pitting and etching during the oxidative leaching. Pits and troughs that have been observed in microbial leaching studies (Berry and Murr, 1978), would increase the effective surface area of the reacted pyrite and hence increase the rate of reaction. Unfortunately, there is no means at the present time to predict the extent of this behaviour or its effects over the long term. It is quite likely that this behaviour occurs only when the pyrite is exposed to highly active oxidation such as in the rapid acid leaching performed in this study and perhaps in microbially catalyzed reactions. At slower leaching rates such as those under alkaline conditions, the trends of the oxidation rates appear to follow the simple SCM with formation of a reaction coating.

The oxidation rates of the fine-grained pyrite and, to a lesser extent, the intermediate grain size follow a more consistent pattern. The former (Fig. 16b), appears to follow the behaviour predicted for diffusion control. This is somewhat surprising because during the acidic oxidation treatment, the iron remains in solution and so should not precipitate to a large degree on the pyrite surfaces. Therefore, the close correspondence with the predicted behaviour would appear to be meaningless in a quantitative sense. It is possible, however, that some reaction coating formed on the pyrite surface especially during the final water wash. If a coating did form and was characterized by a diffusion coefficient that is more consistent with other solids (i.e. 3 to 7 orders-of-magnitude lower than that predicted here) then it is possible to observe this behaviour. It is interesting that the predicted value for De in this case is strikingly similar to those estimated for the long-term runs discussed previously.

CONCLUSIONS

Over extended periods of time, the rate of pyrite oxidation in a dilute alkaline environment decreased by a factor of two or more with time. Experimental evidence suggests that over the course of about one year, resistance to oxidation increases as would occur if a reaction coating were formed on the pyrite surface. When compared to the theoretical behaviour expected for such a process, only slight deviation is observed for the experimental data. The deviation that does occur, however, suggests that the formation of the reaction coating may not be complete or that some of this coating redissolves with time. This results in oxidation rates that are intermediate between those expected for reaction control only and those that are expected when diffusion through the reaction layer is dominant. Because the reduction in rates over the 10 thousand hour experiment was significant, it would seem to be important to include some means of estimating the rate change if predictions of oxidation rates in natural systems are required.

Stages of vigorous oxidative treatment that were used to simulate extended reaction progress resulted in spurious behaviour of the oxidation in the alkaline solution. In one

case, the surface area probably increased during treatment while in another, the reaction rate not only decreased significantly but the observed rates suggest that a surface coating formed. The results do, to some extent, reflect behaviour predicted by the shrinking core model.

The results of the experiment involving the unsaturated reaction cell show that changes in local moisture content do not affect the rate of oxidation when oxygen is in continuous supply. The lack of observable effects on oxidation rates by changing moisture content under the stated conditions suggests that this was not a factor in previous experimental runs. This, hwoever, does not address the question of how oxidation rates would be affected if oxygen were available at only one end of the column. In the case where oxygen would be present only at the surface of a column of pyritic sand for instance, the observed rates would be grately affected by changes in moisture content. The present study suggests only that transport or the resistance to transfer of oxygen between the gas-filled pores and the pyrite surface on the local scale does not change significantly with changes in moisture content.

The rate of solution flow did correlate somewhat with the rate of oxidation probably as a result of changes in the amount of stagnant pore-water in the pyritic sand. Other experiments have shown, however, that this is not a significant factor at slightly higher rates of solution

flow. It is not certain what effect the infiltration rate would have under field conditions.

REFERENCES

Berry, V.K. and Murr, L.E., 1978. Direct observations of bacteria and quantitative studies of their catalytic role in the leaching of low grade, copper-bearing waste. In L.E. Murr, A.E. Torma, and J.A. Brierly (eds.) Metallurgical Applications of Bacterial Leaching and Related Microbiological Phenomena, Academic Press, p. 103-136.

Cherry, J.A.; Gillham, R.W.; Reardon, E.J.; Dubrovsky, N.M. and Nicholson, R.V., 1983. Continuation Study on Hydrogeochemical Processes in Abandoned Uranium Tailings from the Elliot Lake District. WRI Rept. No. 204-02, (CANMET, Energy, Mines and Resourses, Canada) University of Waterloo, 244pp.

Holdren, G.R. and Berner, R.A., 1979. Mechanism of feldspar weathering- I. Experimental studies. Geochim. Cosmochim. Acta, 43:1161-1171.

Levenspiel, O., 1972. Chemical Reaction Engineering, John Wiley, New York, 578 pp.

Appendix A

SUMMARY OF DATA FROM THE LONG-TERM (SURFACE-AREA) EXPERIMENT (PYROX2).

TABLE 5

Summary of sulphate concentrations and effluent weights for PYROX2.

Elapsed time (h)	Effluent Weights (g) / SO_4^{2-} Concentration (mgL^{-1})				
	(1)	(2)	(3)	(4)	(5)
0.	50.3 26.9	50.2 27.2	40.6 26.5	31.9 15.5	31.5 22.8
24.	26.1142.0	94.6 46.7	26.4 96.5	32.2 94.4	63.0 64.8
48.	25.4 96.2	104.2 41.9	45.9 76.2	49.4 72.4	66.7 39.1
120.	3.6100.0	108.5145.0	61.1161.0	198.9 95.5	48.3172.0
144.	95.4147.0	82.3 49.5	193.5 25.9	127.0 27.1	64.6 56.7
168.	56.1158.0	38.3260.0	148.7 53.5	84.9 59.6	61.8 83.1
192.	102.3 76.4	16.1251.0	101.9 67.3	53.3 98.9	43.5 95.5
216.	350.3 17.2	65.0186.0	47.6144.0	106.2 46.0	89.6 41.6
288.	112.2115.0	156.6 28.8	351.4 41.0	89.7105.0	100.4191.0
312.	73.1113.0	142.3 90.9	54.8135.0	94.4107.0	123.1 37.0
336.	205.8 68.0	293.7 42.8	157.5 45.4	237.9 26.3	178.5 34.0
360.	133.5105.0	170.1 64.9	132.5 55.1	183.0 33.0	341.3 14.8
384.	286.3 41.8	88.7127.0	74.3 90.7	121.8 50.5	105.2 47.4
456.	353.4 74.4	192.9118.0	209.8 67.2	209.1 63.3	147.9 74.0
480.	84.5 79.9	122.6 55.0	248.8 18.3	192.9 28.4	120.7 43.7
504.	168.5 61.6	118.6 75.9	84.2 72.0	270.1 14.5	296.8 14.1
528.	277.9 23.1	216.4 41.5	234.7 29.7	42.6 0.0	203.2 19.0
552.	63.0 51.9	144.3 53.7	165.5 38.8	9.4 0.0	162.8 22.8
624.	102.1 74.4	328.7 68.2	499.6 48.0	14.7 0.0	411.9 30.6
672.	501.4 26.6	275.3 63.9	203.7 65.2	1221.6 0.0	121.4 58.2
768.	86.3 18.6	721.2 39.1	640.7 30.7	92.1 41.4	736.5 15.2
864.	572.2 70.5	1304.6 23.8	647.3 27.8	864.8 24.4	496.8 24.3
984.	488.8102.0	541.2 87.7	624.9 50.5	733.6 29.5	254.2 62.3
1056.	244.2125.0	419.0 79.8	250.9 74.6	403.0 22.3	172.0 46.7
1152.	436.4 76.9	482.1 47.8	226.9 78.6	268.9 41.9	246.6 29.5
1224.	238.5115.0	291.2 58.7	399.2 37.9	221.2 38.4	173.9 37.4
1320.	893.6 19.1	640.0 29.5	980.4 18.5	311.8 29.5	335.5 15.6
1392.	62.1323.0	135.2 65.3	186.0 72.2	381.9 17.5	231.7 19.5
1488.	377.5104.0	796.0 20.6	485.3 20.8	616.4 13.9	863.7 9.3
1560.	117.7169.0	114.1 73.4	194.6 71.7	338.4 16.3	427.4 11.3
1656.	139.1193.0	338.3 55.3	605.8 26.1	204.4 37.8	532.3 12.1
1728.	342.1 88.9	130.1110.0	292.3 33.5	536.5 11.6	148.9 23.7
1896.	258.3 87.5	272.8 42.0	923.5 10.0	450.9 11.4	273.5 13.4
1992.	143.7218.0	500.0 39.9	1167.3 8.4	492.3 18.1	421.4 11.7
2064.	552.1 72.3	798.0 14.8	362.6 32.3	602.3 11.7	919.2 4.7
2160.	718.6 73.2	851.8 21.5	693.4 25.9	950.2 10.1	977.1 5.1
2232.	96.5 89.9	100.8 57.0	347.8 17.1	636.8 10.2	166.5 25.6
2328.	278.3210.0	1004.3 19.9	487.3 29.2	854.6 10.8	945.0 6.8
2400.	125.0186.0	541.1 19.2	230.4 36.5	435.6 15.4	287.0 13.1
2496.	595.5 72.8	270.9 40.8	526.9 25.2	581.4 15.0	388.4 15.8
2568.	717.1 47.1	810.2 14.8	834.1 20.1	844.6 6.5	891.8 5.8
2664.	525.9 81.1	942.9 19.5	249.1 43.9	694.6 9.1	408.4 14.6
2736.	113.9177.0	185.3 59.0	445.8 21.9	498.6 9.8	515.3 9.0

2880.	430.8	117.0	933.7	20.4	960.4	15.8	781.2	10.0	809.4	5.7
3072.	586.4	123.0	643.7	38.8	1185.7	28.3	699.7	16.1	1085.6	11.5
3240.	463.2	105.0	907.5	21.1	903.0	19.4	269.0	38.5	1384.2	4.2
3576.	0.0	0.0	0.0	0.0	0.0	0.0	0.0	0.0	0.0	0.0
3744.	576.3	92.2	377.6	56.1	728.9	26.5	727.5	18.4	1143.5	6.9
3912.	491.0	152.0	268.8	68.8	1098.4	12.5	238.3	41.8	438.6	24.0
4080.	892.5	42.3	688.0	27.1	1015.9	0.0	573.2	21.8	973.1	7.5
4584.	0.0	0.0	0.0	0.0	0.0	0.0	0.0	0.0	0.0	0.0
4752.	279.8	165.0	686.5	52.1	1049.0	26.9	864.9	20.4	863.9	14.9
5424.	0.0	0.0	0.0	0.0	0.0	0.0	0.0	0.0	0.0	0.0
5592.	793.0	99.0	668.3	44.7	829.0	28.3	921.3	16.2	844.4	14.9
6432.	0.0	0.0	0.0	0.0	0.0	0.0	0.0	0.0	0.0	0.0
6696.	637.9	147.0	428.7	118.0	1192.8	25.4	1190.4	7.0	1193.7	3.6
6864.	711.2	50.8	661.1	54.9	652.7	48.0	947.3	9.6	977.6	8.3
6936.	620.4	48.2	643.2	28.8	614.5	11.7	488.2	7.8	414.0	9.5
7080.	0.0	0.0	0.0	0.0	0.0	0.0	0.0	0.0	0.0	0.0
7224.	687.3	101.0	923.8	25.2	1193.4	10.5	1191.3	10.4	1030.0	6.8
7392.	1007.4	72.1	1195.3	17.2	1201.9	22.4	889.9	13.6	806.0	12.9
7776.	0.0	0.0	0.0	0.0	0.0	0.0	0.0	0.0	0.0	0.0
7872.	1126.5	34.9	694.1	27.5	908.8	17.9	535.9	13.3	560.0	6.9
8040.	1003.4	56.2	549.2	50.1	387.2	33.7	1195.6	5.0	1021.7	11.3
8208.	737.1	77.1	621.1	34.9	1198.0	11.5	696.6	14.9	725.2	9.4
8352.	1196.5	29.7	1191.6	17.4	1198.4	12.6	940.2	6.9	936.5	15.2
8784.	0.0	0.0	0.0	0.0	0.0	0.0	0.0	0.0	0.0	0.0
8880.	1219.5	26.9	1211.6	13.9	557.9	19.3	1215.6	9.0	772.2	8.0
9048.	1246.5	29.2	992.2	24.5	1036.2	12.9	1246.6	8.8	1181.9	8.5
9120.	1291.5	12.1	1291.6	7.7	963.9	6.4	997.6	4.7	1162.2	4.1
9216.	0.0	0.0	0.0	0.0	0.0	0.0	0.0	0.0	0.0	0.0
9288.	559.2	25.9	664.9	19.2	388.7	14.7	551.2	10.3	1299.2	3.8
9408.	978.3	26.2	1119.0	16.2	125.6	115.0	615.1	9.7	929.6	5.3
9480.	620.4	23.2	1047.6	10.0	1193.4	5.9	1018.6	4.2	816.9	3.7
9624.	339.2	89.6	989.8	19.8	1296.8	9.1	713.0	11.9	1105.1	7.1
9768.	1111.4	34.4	1240.6	21.4	152.2	94.3	156.6	63.9	691.5	23.3
9864.	1043.1	33.0	1186.3	10.0	396.9	29.8	322.2	24.2	412.8	19.6

TABLE 6

Summary of Flow Rate Data for the Preliminary Surface Area Experiment (PYROX2).

Date	Hour	Collection Time (h)	Average Flow Rates ($mL\ h^{-1}$)				
			(1)	(2)	(3)	(4)	(5)
821202	24.	24.	1.1	3.9	1.1	1.3	2.6
821203	48.	24.	1.1	4.3	1.9	2.1	2.8
821206	120.	72.	0.1	1.5	0.8	2.8	0.7
821207	144.	24.	4.0	3.4	8.1	5.3	2.7
821208	168.	24.	2.3	1.6	6.2	3.5	2.6
821209	192.	24.	4.3	0.7	4.2	2.2	1.8
821210	216.	24.	14.6	2.7	2.0	4.4	3.7
821213	288.	72.	1.6	2.2	4.9	1.2	1.4
821214	312.	24.	3.0	5.9	2.3	3.9	5.1
821215	336.	24.	8.6	12.2	6.6	9.9	7.4
821216	360.	24.	5.6	7.1	5.5	7.6	14.2
821217	384.	24.	11.9	3.7	3.1	5.1	4.4
821220	456.	72.	4.9	2.7	2.9	2.9	2.1
821221	480.	24.	3.5	5.1	10.4	8.0	5.0
821222	504.	24.	7.0	4.9	3.5	11.3	12.4
821223	528.	24.	11.6	9.0	9.8	1.8	8.5
821224	552.	24.	2.6	6.0	6.9	0.4	6.8
821227	624.	72.	1.4	4.6	6.9	0.2	5.7
821229	672.	48.	10.4	5.7	4.2	25.4	2.5
830102	768.	96.	0.9	7.5	6.7	1.0	7.7
830106	864.	96.	6.0	13.6	6.7	9.0	5.2
830111	984.	120.	4.1	4.5	5.2	6.1	2.1
830114	1056.	72.	3.4	5.8	3.5	5.6	2.4
830118	1152.	96.	4.5	5.0	2.4	2.8	2.6
830121	1224.	72.	3.3	4.0	5.5	3.1	2.4
830125	1320.	96.	9.3	6.7	10.2	3.2	3.5
830128	1392.	72.	0.9	1.9	2.6	5.3	3.2
830201	1488.	96.	3.9	8.3	5.1	6.4	9.0
830204	1560.	72.	1.6	1.6	2.7	4.7	5.9
830208	1656.	96.	1.4	3.5	6.3	2.1	5.5
830211	1728.	72.	4.8	1.8	4.1	7.5	2.1
830218	1896.	168.	1.5	1.6	5.5	2.7	1.6
830222	1992.	96.	1.5	5.2	12.2	5.1	4.4
830225	2064.	72.	7.7	11.1	5.0	8.4	12.8
830301	2160.	96.	7.5	8.9	7.2	9.3	10.2
830304	2232.	72.	1.3	1.4	4.8	8.8	2.3
830308	2328.	96.	2.9	10.5	5.1	8.9	9.8
830311	2400.	72.	1.7	7.5	3.2	6.0	4.0
830315	2496.	96.	6.2	2.8	5.5	6.1	4.0
830318	2568.	72.	10.0	11.3	11.6	11.7	12.4
830322	2664.	96.	5.5	9.8	2.6	7.2	4.3
830325	2736.	72.	1.6	2.6	6.2	6.9	7.2
830331	2880.	144.	3.0	6.5	6.7	5.4	5.6
830408	3072.	192.	3.1	3.4	6.2	3.6	5.7

830415	3240.	168.	2.8	5.4	5.4	1.6	8.2
830429	3576.	336.	0.0	0.0	0.0	0.0	0.0
830506	3744.	168.	3.4	2.2	4.3	4.3	6.8
830513	3912.	168.	2.9	1.6	6.5	1.4	2.6
830520	4080.	168.	5.3	4.1	6.0	3.4	5.8
830610	4584.	504.	0.0	0.0	0.0	0.0	0.0
830617	4752.	168.	1.7	4.1	6.2	5.1	5.1
830715	5424.	672.	0.0	0.0	0.0	0.0	0.0
830722	5592.	168.	4.7	4.0	4.9	5.5	5.0
830826	6432.	840.	0.0	0.0	0.0	0.0	0.0
830906	6696.	264.	2.4	1.6	4.5	4.5	4.5
830913	6864.	168.	4.2	3.9	3.9	5.6	5.8
830916	6936.	72.	8.6	8.9	8.5	6.8	5.8
830922	7080.	144.	0.0	0.0	0.0	0.0	0.0
830928	7224.	144.	4.8	6.4	8.3	8.3	7.2
831005	7392.	168.	6.0	7.1	7.2	5.3	4.8
831021	7776.	384.	0.0	0.0	0.0	0.0	0.0
831025	7872.	96.	11.7	7.2	9.5	5.6	5.8
831101	8040.	168.	6.0	3.3	2.3	7.1	6.1
831108	8208.	168.	4.4	3.7	7.1	4.1	4.3
831114	8352.	144.	8.3	8.3	8.3	6.5	6.5
831202	8784.	432.	0.0	0.0	0.0	0.0	0.0
831206	8880.	96.	12.7	12.6	5.8	12.7	8.0
831213	9048.	168.	7.4	5.9	6.2	7.4	7.0
831216	9120.	72.	17.9	17.9	13.4	13.9	16.1
831220	9216.	96.	0.0	0.0	0.0	0.0	0.0
831223	9288.	72.	7.8	9.2	5.4	7.7	18.0
831228	9408.	120.	8.2	9.3	1.0	5.1	7.7
831231	9480.	72.	8.6	14.5	16.6	14.1	11.3
840106	9624.	144.	2.4	6.9	9.0	5.0	7.7
840112	9768.	144.	7.7	8.6	1.1	1.1	4.8
840116	9864.	96.	10.9	12.4	4.1	3.4	4.3

TABLE 7

Summary of Average Oxidation Rates for the Preliminary Surface Area experiment (PYROX2).

Date	Hour	Collect Time (h)	Average Oxidation Rates ($mol\text{-}FeS_2\ h^{-1}\ g^{-1}$) (1)	(2)	(3)	(4)	(5)
821201	0.		0.352E-06	0.355E-06	0.280E-06	0.129E-06	0.187E-06
821202	24.	24.	0.402E-07	0.479E-07	0.276E-07	0.330E-07	0.443E-07
821203	48.	24.	0.265E-07	0.474E-07	0.379E-07	0.388E-07	0.283E-07
821206	120.	72.	0.130E-08	0.569E-07	0.356E-07	0.687E-07	0.300E-07
821207	144.	24.	0.152E-06	0.442E-07	0.544E-07	0.373E-07	0.397E-07
821208	168.	24.	0.961E-07	0.108E-06	0.863E-07	0.549E-07	0.557E-07
821209	192.	24.	0.848E-07	0.438E-07	0.744E-07	0.572E-07	0.451E-07
821210	216.	24.	0.653E-07	0.131E-06	0.743E-07	0.530E-07	0.404E-07
821213	288.	72.	0.466E-07	0.163E-07	0.521E-07	0.341E-07	0.693E-07
821214	312.	24.	0.896E-07	0.140E-06	0.802E-07	0.110E-06	0.494E-07
821215	336.	24.	0.152E-06	0.136E-06	0.776E-07	0.679E-07	0.658E-07
821216	360.	24.	0.152E-06	0.120E-06	0.792E-07	0.655E-07	0.548E-07
821217	384.	24.	0.130E-06	0.122E-06	0.731E-07	0.667E-07	0.541E-07
821220	456.	72.	0.951E-07	0.823E-07	0.510E-07	0.479E-07	0.396E-07
821221	480.	24.	0.732E-07	0.731E-07	0.494E-07	0.594E-07	0.572E-07
821222	504.	24.	0.113E-06	0.976E-07	0.658E-07	0.425E-07	0.454E-07
821223	528.	24.	0.696E-07	0.974E-07	0.756E-07	0.000E 00	0.419E-07
821224	552.	24.	0.355E-07	0.840E-07	0.696E-07	0.000E 00	0.403E-07
821227	624.	72.	0.275E-07	0.810E-07	0.867E-07	0.000E 00	0.456E-07
821229	672.	48.	0.723E-07	0.954E-07	0.720E-07	0.000E 00	0.383E-07
830102	768.	96.	0.435E-08	0.765E-07	0.533E-07	0.103E-07	0.304E-07
830106	864.	96.	0.109E-06	0.842E-07	0.488E-07	0.572E-07	0.327E-07
830111	984.	120.	0.108E-06	0.103E-06	0.685E-07	0.469E-07	0.344E-07
830114	1056.	72.	0.110E-06	0.121E-06	0.677E-07	0.325E-07	0.290E-07
830118	1152.	96.	0.910E-07	0.625E-07	0.484E-07	0.305E-07	0.197E-07
830121	1224.	72.	0.992E-07	0.618E-07	0.547E-07	0.307E-07	0.235E-07
830125	1320.	96.	0.463E-07	0.512E-07	0.492E-07	0.249E-07	0.142E-07
830128	1392.	72.	0.725E-07	0.319E-07	0.486E-07	0.242E-07	0.163E-07
830201	1488.	96.	0.106E-06	0.445E-07	0.274E-07	0.232E-07	0.217E-07
830204	1560.	72.	0.719E-07	0.303E-07	0.504E-07	0.199E-07	0.175E-07
830208	1656.	96.	0.728E-07	0.507E-07	0.429E-07	0.209E-07	0.175E-07
830211	1728.	72.	0.110E-06	0.517E-07	0.354E-07	0.225E-07	0.128E-07
830218	1896.	168.	0.350E-07	0.178E-07	0.143E-07	0.796E-08	0.568E-08
830222	1992.	96.	0.849E-07	0.541E-07	0.266E-07	0.242E-07	0.134E-07
830225	2064.	72.	0.144E-06	0.427E-07	0.423E-07	0.255E-07	0.156E-07
830301	2160.	96.	0.143E-06	0.497E-07	0.487E-07	0.260E-07	0.135E-07
830304	2232.	72.	0.314E-07	0.208E-07	0.215E-07	0.235E-07	0.154E-07
830308	2328.	96.	0.158E-06	0.542E-07	0.386E-07	0.250E-07	0.174E-07
830311	2400.	72.	0.841E-07	0.376E-07	0.304E-07	0.243E-07	0.136E-07
830315	2496.	96.	0.118E-06	0.300E-07	0.360E-07	0.236E-07	0.166E-07
830318	2568.	72.	0.122E-06	0.434E-07	0.606E-07	0.198E-07	0.187E-07
830322	2664.	96.	0.116E-06	0.499E-07	0.297E-07	0.171E-07	0.162E-07
830325	2736.	72.	0.729E-07	0.395E-07	0.353E-07	0.177E-07	0.168E-07
830331	2880.	144.	0.911E-07	0.344E-07	0.274E-07	0.141E-07	0.834E-08

830408	3072.	192.	0.978E-07	0.339E-07	0.455E-07	0.153E-07	0.169E-07
830415	3240.	168.	0.754E-07	0.297E-07	0.271E-07	0.160E-07	0.901E-08
830429	3576.	336.	0.000E 00	0.000E 00	0.000E 00	0.000E 00	0.000E 00
830506	3744.	168.	0.823E-07	0.328E-07	0.299E-07	0.207E-07	0.122E-07
830513	3912.	168.	0.116E-06	0.287E-07	0.213E-07	0.154E-07	0.163E-07
830520	4080.	168.	0.585E-07	0.289E-07	0.000E 00	0.194E-07	0.113E-07
830610	4584.	504.	0.000E 00	0.000E 00	0.000E 00	0.000E 00	0.000E 00
830617	4752.	168.	0.715E-07	0.554E-07	0.437E-07	0.273E-07	0.199E-07
830715	5424.	672.	0.000E 00	0.000E 00	0.000E 00	0.000E 00	0.000E 00
830722	5592.	168.	0.122E-06	0.463E-07	0.364E-07	0.231E-07	0.195E-07
830826	6432.	840.	0.000E 00	0.000E 00	0.000E 00	0.000E 00	0.000E 00
830906	6696.	264.	0.925E-07	0.499E-07	0.299E-07	0.822E-08	0.424E-08
830913	6864.	168.	0.560E-07	0.562E-07	0.485E-07	0.141E-07	0.126E-07
830916	6936.	72.	0.108E-06	0.670E-07	0.260E-07	0.138E-07	0.142E-07
830922	7080.	144.	0.000E 00	0.000E 00	0.000E 00	0.000E 00	0.000E 00
830928	7224.	144.	0.125E-06	0.421E-07	0.227E-07	0.224E-07	0.127E-07
831005	7392.	168.	0.113E-06	0.319E-07	0.417E-07	0.188E-07	0.161E-07
831021	7776.	384.	0.000E 00	0.000E 00	0.000E 00	0.000E 00	0.000E 00
831025	7872.	96.	0.107E-06	0.518E-07	0.441E-07	0.193E-07	0.105E-07
831101	8040.	168.	0.874E-07	0.426E-07	0.202E-07	0.926E-08	0.179E-07
831108	8208.	168.	0.881E-07	0.336E-07	0.213E-07	0.161E-07	0.106E-07
831114	8352.	144.	0.642E-07	0.375E-07	0.273E-07	0.117E-07	0.257E-07
831202	8784.	432.	0.000E 00	0.000E 00	0.000E 00	0.000E 00	0.000E 00
831206	8880.	96.	0.889E-07	0.457E-07	0.292E-07	0.297E-07	0.168E-07
831213	9048.	168.	0.564E-07	0.377E-07	0.207E-07	0.170E-07	0.156E-07
831216	9120.	72.	0.565E-07	0.360E-07	0.223E-07	0.170E-07	0.172E-07
831220	9216.	96.	0.000E 00	0.000E 00	0.000E 00	0.000E 00	0.000E 00
831223	9288.	72.	0.524E-07	0.462E-07	0.207E-07	0.205E-07	0.178E-07
831228	9408.	120.	0.556E-07	0.393E-07	0.313E-07	0.129E-07	0.107E-07
831231	9480.	72.	0.520E-07	0.379E-07	0.255E-07	0.155E-07	0.109E-07
840106	9624.	144.	0.549E-07	0.354E-07	0.213E-07	0.153E-07	0.142E-07
840112	9768.	144.	0.691E-07	0.480E-07	0.259E-07	0.181E-07	0.291E-07
840116	9864.	96.	0.933E-07	0.322E-07	0.321E-07	0.211E-07	0.219E-07

Unit numbers refer to grain-size diameters:

(1) = 54
(2) = 76
(3) = 108
(4) = 153
(5) = 215

Appendix B

SUMMARY OF THE DATA FROM THE SIMULATED REACTION PROGRESS EXPERIMENT (PYROX10)

TABLE 8

Summary of the average flow rates for the PYROX10 series experiment

Date	Time (h)	Collection Interval (h)	Flow Rates (mL h^{-1})					
			(1a)	(1b)	(2a)	(2b)	(3a)	(3b)
840425	0.							
840425	4.	4.	18.6	28.0	18.6	30.1	11.6	25.2
840426	23.	19.	9.7	12.9	17.2	6.7	9.2	9.4
840426	30.	7.	17.0	19.0	27.6	18.8	15.9	22.6
840427	47.	17.	9.0	9.3	17.2	9.3	8.6	11.0
840504	239.	192.	0.0	0.0	0.0	0.0	0.0	0.0
840507	313.	75.	1.7	1.2	1.4	1.0	1.0	0.5
840507	318.	5.	0.0	0.0	0.0	0.0	0.0	0.0
840508	334.	15.	16.0	13.7	19.1	13.5	12.4	5.9
840508	0.							
840509	23.	23.	2.1	6.5	7.0	2.6	1.2	4.4
840510	42.	19.	5.3	4.4	8.9	3.8	3.2	5.8
840510	48.	6.	2.8	10.9	5.9	2.1	7.6	3.2
840511	66.	17.	2.5	8.5	4.3	1.4	2.0	1.8
840514	80.	15.	0.0	0.0	0.0	0.0	0.0	0.0
840514	87.	7.	9.3	13.8	13.2	4.8	9.6	7.9
840515	104.	17.	8.2	17.4	7.5	3.6	12.0	9.1
840515	0.							
840516	25.	25.	9.2	8.9	2.5	2.0	1.4	3.5
840516	31.	6.	9.1	11.7	18.0	14.6	17.6	9.1
840517	49.	18.	3.2	5.4	7.0	4.2	3.6	4.3
840518	71.	22.	2.4	5.8	6.0	3.0	1.4	2.9
840519	105.	34.	0.0	0.0	0.0	0.0	0.0	0.0
840520	129.	24.	5.8	2.7	10.0	0.9	3.4	0.4
840522	169.	40.	5.4	3.4	2.7	0.4	4.1	3.8
840523	190.	22.	7.7	2.4	2.6	5.4	3.4	1.8
840523	0.							
840524	26.	26.	6.9	11.7	11.5	2.4	1.6	5.2
840524	31.	6.	11.1	22.2	21.6	13.6	10.7	14.8
840525	50.	19.	6.6	11.3	13.7	7.8	3.2	10.1
840525	55.	5.	10.3	19.8	22.7	11.7	5.0	16.2
840528	120.	65.	0.0	0.0	0.0	0.0	0.0	0.0
840528	127.	7.	23.1	12.8	10.8	6.6	14.3	20.5
840529	145.	18.	15.5	5.6	4.1	7.1	5.8	8.3
840529	0.							
840530	23.	23.	7.9	8.9	13.2	12.6	1.7	13.0
840530	30.	8.	6.2	8.4	22.5	16.0	6.4	17.1
840531	48.	18.	12.8	4.5	8.1	11.0	5.9	8.6
840531	54.	7.	11.0	10.1	11.7	19.6	6.1	13.2
840601	71.	17.	14.1	6.4	4.2	9.9	2.1	5.9
840604	0.							
840605	31.	31.	2.6	4.1	9.0	2.9	4.9	3.1
840606	48.	17.	9.8	16.2	17.5	11.4	14.3	10.2
840606	57.	9.	14.9	10.6	12.8	8.3	9.3	3.5

840607	71.	15.	21.2	9.2	10.0	10.6	12.2	3.8
840607	79.	7.	20.8	23.4	29.9	15.2	11.2	16.0
840608	96.	17.	7.2	8.8	10.8	5.4	3.3	4.9

TABLE 9

Summary of the oxidation rates for the PYROX10 series experiment.

Date	Time (h)	Collection Interval (h)	Oxidation Rate ($mol\text{-}FeS_2\ h^{-1}$)					
			(1a)	(1b)	(2a)	(2b)	(3a)	(3b)
840425	0.							
840425	4.	4.	0.541E-07	0.569E-07	0.211E-06	0.199E-06	0.312E-06	0.185E-06
840426	23.	19.	0.172E-07	0.189E-07	0.574E-07	0.420E-07	0.109E-06	0.858E-07
840426	30.	7.	0.230E-07	0.208E-07	0.647E-07	0.529E-07	0.124E-06	0.119E-06
840427	47.	17.	0.168E-07	0.174E-07	0.572E-07	0.427E-07	0.121E-06	0.123E-06
840504	239.	192.	0.000E 00	0.000E 00	0.000E 00	0.000E 00	0.000E 00	0.000E 00
840507	313.	75.	0.127E-08	0.116E-08	0.257E-08	0.201E-08	0.868E-08	0.812E-08
840507	318.	5.	0.000E 00	0.000E 00	0.000E 00	0.000E 00	0.000E 00	0.000E 00
840508	334.	15.	0.133E-07	0.157E-07	0.309E-07	0.260E-07	0.124E-06	0.106E-06
840508	0.							
840509	23.	23.	0.477E-08	0.713E-08	0.480E-07	0.188E-07	0.943E-08	0.833E-08
840510	42.	19.	0.149E-07	0.197E-07	0.451E-07	0.407E-07	0.418E-07	0.323E-07
840510	48.	6.	0.169E-07	0.249E-07	0.494E-07	0.453E-07	0.543E-07	0.567E-07
840511	66.	17.	0.161E-07	0.230E-07	0.466E-07	0.442E-07	0.568E-07	0.580E-07
840514	80.	15.	0.000E 00	0.000E 00	0.000E 00	0.000E 00	0.000E 00	0.000E 00
840514	87.	7.	0.189E-07	0.309E-07	0.455E-07	0.491E-07	0.734E-07	0.702E-07
840515	104.	17.	0.162E-07	0.226E-07	0.436E-07	0.352E-07	0.733E-07	0.709E-07
840515	0.							
840516	25.	25.	0.110E-07	0.345E-07	0.215E-07	0.324E-07	0.346E-07	0.413E-07
840516	31.	6.	0.989E-08	0.140E-07	0.376E-07	0.114E-07	0.247E-07	0.288E-07
840517	49.	18.	0.487E-08	0.174E-07	0.990E-08	0.744E-08	0.235E-07	0.301E-07
840518	71.	22.	0.496E-08	0.213E-07	0.112E-07	0.799E-08	0.239E-07	0.326E-07
840519	105.	34.	0.000E 00	0.000E 00	0.000E 00	0.000E 00	0.000E 00	0.000E 00
840520	129.	24.	0.786E-08	0.201E-07	0.162E-07	0.114E-07	0.387E-07	0.348E-07
840522	169.	40.	0.151E-07	0.208E-07	0.172E-07	0.657E-08	0.466E-07	0.512E-07
840523	190.	22.	0.136E-07	0.251E-07	0.272E-07	0.152E-07	0.542E-07	0.581E-07
840523	0.							
840524	26.	26.	0.158E-07	0.188E-07	0.292E-07	0.543E-07	0.745E-07	0.751E-07
840524	31.	6.	0.924E-08	0.277E-07	0.237E-07	0.412E-07	0.534E-07	0.331E-07
840525	50.	19.	0.583E-08	0.135E-07	0.350E-07	0.934E-08	0.226E-07	0.257E-07
840525	55.	5.	0.807E-08	0.185E-07	0.603E-07	0.134E-07	0.554E-07	0.372E-07
840528	120.	65.	0.000E 00	0.000E 00	0.000E 00	0.000E 00	0.000E 00	0.000E 00
840528	127.	7.	0.156E-07	0.254E-07	0.186E-07	0.489E-07	0.677E-07	0.652E-07
840529	145.	18.	0.971E-08	0.135E-07	0.103E-07	0.103E-07	0.158E-07	0.224E-07
840529	0.							
840530	23.	23.	0.229E-07	0.297E-07	0.357E-07	0.250E-07	0.513E-07	0.521E-07
840530	30.	8.	0.228E-07	0.145E-07	0.187E-07	0.357E-07	0.225E-07	0.293E-07
840531	48.	18.	0.120E-07	0.444E-07	0.136E-07	0.177E-07	0.173E-07	0.191E-07
840531	54.	7.	0.160E-07	0.262E-07	0.245E-07	0.163E-07	0.229E-07	0.241E-07
840601	71.	17.	0.103E-07	0.174E-07	0.135E-07	0.103E-07	0.183E-07	0.107E-07
840604	0.							
840605	31.	31.	0.321E-08	0.655E-08	0.892E-08	0.130E-07	0.785E-08	0.501E-08

840606	48.	17.	0.143E-07	0.270E-07	0.209E-07	0.183E-07	0.261E-07	0.212E-07
840606	57.	9.	0.140E-07	0.293E-07	0.233E-07	0.160E-07	0.238E-07	0.219E-07
840607	71.	15.	0.287E-07	0.394E-07	0.350E-07	0.237E-07	0.386E-07	0.488E-07
840607	79.	7.	0.216E-07	0.499E-07	0.435E-07	0.253E-07	0.859E-07	0.407E-07
840608	96.	17.	0.139E-07	0.279E-07	0.203E-07	0.252E-07	0.279E-07	0.250E-07

Unit numbers refer to grain-size diameters (in microns), a and b are replicates.

(1)=215
(2)=108
(3)= 54